Composites Part B 164 (2019) 720–731

Contents lists available at ScienceDirect

Composites Part B

journal homepage: www.elsevier.com/locate/compositesb

Improving damping property of carbon-fiber reinforced epoxy composite through novel hybrid epoxy-polyurea interfacial reaction

Thomas L. Attard[a], Li He[a], Hongyu Zhou[b,*]

[a] Department of Civil and Environmental Engineering, University of Alabama at Birmingham, AL, 35294, USA
[b] Department of Civil and Environmental Engineering, University of Alabama in Huntsville, AL, 35899, USA

ARTICLE INFO

Keywords:
Hybrid polymer matrix composite
Vibration
Internal friction/Damping
Polyurea

ABSTRACT

A **C**arbon-fiber reinforced **H**ybrid- **M**atrix **C**omposite (CHMC) was designed to improve the material damping property in conventional carbon-fiber reinforced epoxy (CF/E) through the interfacial reaction of two reactive polymeric compounds: still-curing epoxy-based phase I with a highly crosslinked morphology and lightly crosslinked still-curing polyurea elastomeric phase II. Chemical reactions of the hybridized interfacial matrix are discussed relative to phase reactions and tunable material damping in accordance with the migration of epoxy phase I species. Microstructures and micromechanical properties of CHMC are characterized using scanning electron microscopy and nanoindentation. Dynamic properties of CHMC are investigated via free vibration and forced vibration tests, and the results are compared to CF/E test results. Dynamic mechanical analysis reveals a cogent link between damping property (of the epoxy-polyurea interface) and lower $t_c \approx 0$, where proper design of the epoxy-polyurea interface can greatly improve material damping by using smaller epoxy curing times (t_c, hours) just before topically applying reactive polyurea. As a result, loss modulus of the interface is seven to ten times larger for $t_c = 0$ compared to polyurea-coated fully-cured epoxy. For $t_c > 3.5$, the role of polyurea thickness h_p on energy dissipation expectedly increases.

1. Introduction

Material damping is a vital design component in the control of vibrations in various types of structural dynamics applications. A few benefits of incorporating materials with enhanced damping in structural design include: extending service life of components, attenuating acceleration and displacement responses, reducing noise, and possible reduction of total structural weight. In general, polymeric matrix composites (PMCs) provide higher material damping than metallic materials, where energy dissipation within fibrous composites may be attributed to: (1) viscoelastic/viscoplastic nature of the fiber and matrix constituents; (2) interaction between material phases; and/or (3) material damage in pre-existing or new structures [1]. At the laminate level, the damping ratio of fibrous composites depends not only on the constituent lamina (or ply) properties, but also on ply orientations and inter-laminar effects [2–4].

Early experimental studies on damping properties of fiber-reinforced composite include the works of Adams and his colleagues [5,6]. In their experiments, beam specimens were excited in free-free mode of vibration using a coil/electromagnet driver transducer. The excitation signal was tuned to the fundamental natural frequency of the beam, where damping of the composite beams was quantified by calculating energy input per cycle during steady-state vibration modes. Gibson and Plunkett [7], Suarez et al. [8,9], and Crane and Gillespie [10] used an impulse method to evaluate damping of composite materials, where impulsive excitation was induced to flat cantilever beam specimens using an electromagnetic hammer. Transverse beam displacements were measured using a non-contact eddy current probe positioned near the tip of the beam. The frequency response function was obtained using a Fourier transform of the measured time-history data, and the materials' loss factor and complex modulus were evaluated by curve fitting to the results of the Fourier transform. Using the same approach, Hadi and Ashton [11] evaluated damping of glass fiber-reinforced epoxies using free vibration response of cantilever beams via logarithmic decrement fitting. More recently, damping of carbon nanotube composites [12,13] was evaluated using random excitation and sinusoidal sweep tests. Additionally, several studies have examined developing damping models for fibrous composites, including Ludwig et al. [14] who developed a linear viscoelastic model to predict the damped response and energy transfer in laminated composite structures subjected to dynamic excitations. Liu et al. [15] predicted damping and progressive failure mechanisms in composite materials using

* Corresponding author. 5000, Tech. Drive, Huntsville, AL, USA.
E-mail address: hongyu.zhou@uah.edu (H. Zhou).

https://doi.org/10.1016/j.compositesb.2019.01.064
Received 15 July 2018; Received in revised form 12 January 2019; Accepted 21 January 2019
Available online 23 January 2019
1359-8368/

approximate strain localizations. A deeper treatment of micro-macro interfacial models for stiffness and damping matrices was provided by Hwang and Gibson [16] using an energy-based finite element analysis of fiber/matrix interphase size, inter-laminar stress, and fiber orientation.

While it may appear contradictory to be able to integrate high-stiffness and high-damping within a single material system in structural design [17], hierarchical microstructures of composite materials give rise to combined high-stiffness and high-damping, i.e., material systems comprised of a stiff, low damping phase (e.g., reinforcing fiber) and a compliant, high damping phase (e.g., binding matrix and additives). Previous studies [18,19] have shown that inclusion of soft particulate phases, such as core-shell rubber (CSR), into epoxy-based matrices can improve damping but may also reduce elastic modulus while introducing defects at the 'rigid-epoxy-matrix/rubber' boundary due to low bond enthalpy and surface energy in immiscible admixtures. Similarly, additives such as nano-graphene and carbon-nanotubes (CNTs) can effectively increase material damping due to a “stick-slip" mechanism [13]. However, potential drawbacks of using nano-particles include their tendency to agglomerate, which would in-turn change matrix rheological properties. To be able to circumvent some of these limitations, a tunable **C**arbon-fiber reinforced **H**ybrid-**M**atrix **C**omposite, or CHMC, was recently developed to dial-in high material damping while maintaining sufficient stiffness of the composite material system. CHMC was created by introducing a designable pre-polymerized isocyanate-amine system, i.e., a highly reactive polyurea, to a curing epoxy network - a typical matrix binder for fibrous composites. The outcome is a tunable pre-polymerized isocyanate-amine/epoxide interfacial reaction, where properties such as fracture toughness and damping may be fine-tuned based on the reaction kinetics of the reacting polymers.

The new hybridized polymeric matrix interface integrates high-stiffness and good fiber saturation within lightly crosslinked elastomers, engendering high-damping and high fracture toughness. Recent studies conducted by Zhou and Attard [20] and Zhou et al. [21] utilized CHMC as a structural retrofitting material, able to sustain high mechanical strength in the otherwise brittle carbon-fiber reinforced epoxy (CF/E) composite. In this research, dynamic properties (i.e., damping ratio and complex moduli) of CHMC are experimentally tested under free-vibration and randomly-excited forced vibration. The chemical reactions of the interfacial region between the reactive polyurea and epoxy are discussed; microstructures of CHMC were characterized using scanning electron microscopy (SEM), and micromechanical properties of each constituent phase within CHMC were tested using nanoindentation. Test results were compared to those obtained from conventional carbon fiber reinforced epoxy composite. Finally, a comparison of three values of elapsed curing time, t_c, used to design the interfacial region, reveals that lower t_c has a profound effect on the design of damping in CHMC structures.

2. The carbon-fiber reinforced hybrid matrix composite (CHMC)

The strength and stiffness of continuous fiber composites are mostly governed by fiber properties while matrix phases provide stress transferring paths for reinforcing fibers, making the matrix phases responsible for fracture toughness and energy absorption/transfer (“dissipation”) properties [22]. Most thermosetting polymers, such as epoxies, fracture at relatively low ultimate strains. Consequently, damage events that initiate at the fiber-matrix interface quickly bridge together via matrix cracking, causing failure to the composite material system. In order to improve the damage tolerance of polymeric composites, “damage barriers” may be introduced to the composite to isolate microscopic damage events, rendering individual cracks harmless. Fig. 1(c)–(f) show the results of SEM images of a multilayered cross-ply morphology of CHMC, where reinforcing carbon fibers are well-saturated in an epoxy matrix phase I, followed by surface-level application of an elastomeric pre-polymerized polyurea matrix phase II (with rapid curing); the term ‘pre-polymerized’ indicates the ongoing reactivity, of the isocyanate and amine functional groups that comprise polyurea. Interfacial chemical reactions of CHMC include pre-polymerized polyurea and curing epoxy, where width of the interface region varies between 2 μm and 50 μm (Fig. 1 (f)), depending on how long (t_c) the two-part epoxy had been curing upon surface-coating it with pre-polymerized polyurea. Depending on t_c (and to lesser extent, the overlying thickness of polyurea, h_p), composite action and overall CHMC damping between the adjoined fibrous lamina and overlying polyurea are controlled via molecular mobility of the hybridized interface.

The hybridized interface dials-in material energy dissipation as a function of the elapsed curing time, t_c, of the epoxy network whose epoxide and hydroxyl (−OH) functional groups react with the functional groups of pre-polymerized polyurea, i.e., reactive isocyanate (−NCO) and amine-based ($-NH_2$). The variable t_c may be used to tune the interfacial width, chemical bonds, and molecular mobility of the interface (via molecular vibration modes) in order to design damping and composite action within CHMC. Following the interfacial, or surface, application of pre-polymerized polyurea, polyurea continues to be applied, quickly curing (often in less than 1 min) to form a top layer of thickness, $\boldsymbol{h_p}$, see Fig. 1 (c).

The epoxy matrix phase I is synthesized by condensation polymerization, crosslinking a resin molecule via ring-opening, with a wide range of hardeners, including amines, acids, phenols, and alcohols, to form an epoxy structure. In this study, diglycidyl ether of bisphenol A (DGEBA) and polyetheramine are chosen as the resin and hardener, respectively. The DGEBA molecule is first synthesized by epichlorohydrin (ECH) and bisphenol A (BPA). The polyetheramine hardener, containing highly reactive amine functional groups ($-NH_2$), enhances exothermic reactivity and facilitates epoxy crosslinking, see Fig. 2 (a). At time t_c, the crosslinking of curing DGEBA - polyetheramine reaction is surface-interrupted by applying pre-polymerized polyurea, see Fig. 2 (b). Pre-polymerized polyurea is mixed at a 1:1 ratio (by volume) of Part A (−NCO-based) to Part B ($-NH_2$-based), where Part A for aliphatic systems is based on isophorone diisocyanate (IPDI) and Part B is the more complex resin-blend component that consists of amine-based resins and chain extenders. Away from the epoxy-polyurea interface, the ($-NH_2$) and (−NCO) functional groups polymerize in less than 90 s to produce a pure polyurea phase II.

To limit moisture at the interface, aliphatic systems, which do not include polyol as in aromatic systems, were used in the study. A series of experiments was conducted to deduce a likely reaction between polyurea and epoxy moieties. No reaction was observed in the following mixtures: (−NCO) with epoxide, ($-NH_2$-polyurea) with epoxide, and (−NCO) with (−OH) from the DGEBA backbone. However, a mixture of (epoxide) + (amine epoxy hardener) + (isocyanate), which solidifies in seconds after mixing, is a likely three-part reaction that produces an epoxy-urea bond and comprises the new interfacial chemical structure in Fig. 2 (c). By controlling migration patterns of the epoxy groups via t_c, the interface, consisting of a denser distribution of covalently bonded structures at lower t_c, e.g., 0 h or 0.5 h, and minimal gapping, may be designed to enhance energy transferability (for example through material damping) and thus control vibrations in stand-alone or reinforced substrates, for example, steel beams.

3. Characterization of viscous and elastic properties using nanoindentation

3.1. Nanoindentation test of constituent phases within CHMC

In order to evaluate the frequency and damping response of CHMC laminates, material properties of the CHMC constituents were tested using a *Hysitron Tribo-indentor*. The analysis of load-penetration curves is in accordance with Oliver and Pharr [23], where reduced elastic modulus, E_r, of the testing material is related to the slope of the unloading curve initiated at maximum load point, $S|_{Pmax}$, Fig. 3(a), as

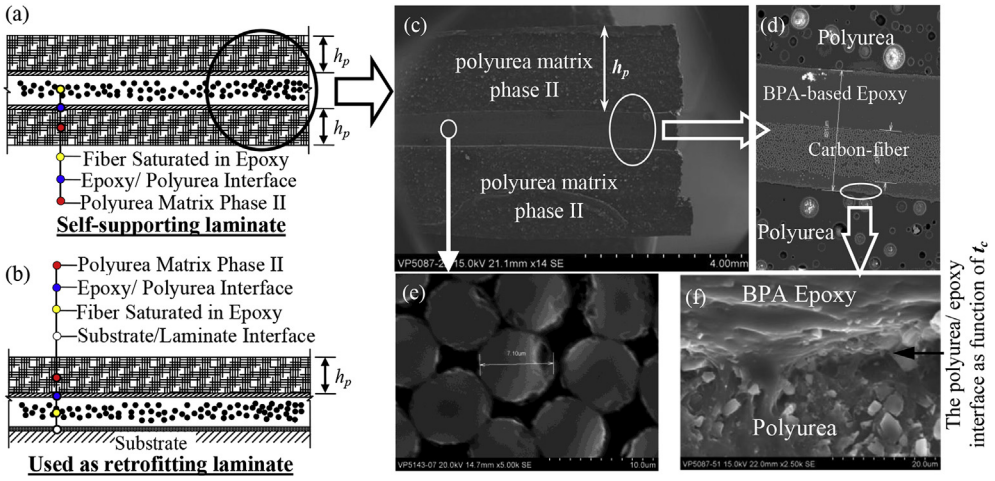

Fig. 1. Illustrative figure showing the multilayered cross-ply layout of CHMC: (a) stand-alone system; (b) used as a retrofitting material to a substrate; (c) SEM image showing microstructures of the CHMC; (d) a close-up view of reinforcing fiber and hybrid matrix system of CHMC; (e) reinforcing carbon fiber embedded in the cured epoxy; (f) close-up view of the polyurea/epoxy interface.

$$E_r = \frac{\sqrt{\pi}}{2\beta}\frac{S|_{P_{\max}}}{\sqrt{A_p(h_c)}} \tag{1}$$

where $A_p(h_c)$ is the projected area of tip-sample contact at the contact depth h_c, see Fig. 3(b), and where a Berkovich tip is used to perform the indentation tests; and β is a factor to account for the geometrical shape of the indentor tip [23]. The Young's modulus of the testing sample, E_s, may then be calculated using Equation (7) as:

$$\frac{1}{E_r} = \frac{(1-\upsilon_s^2)}{E_s} + \frac{(1-\upsilon_i^2)}{E_i} \tag{2}$$

where E_i and ν_i are Young's modulus and Poisson's ratio of the indentor tip; and ν_s is the Young's modulus of the testing sample.

The nanoindentation relationships for each of the three primary

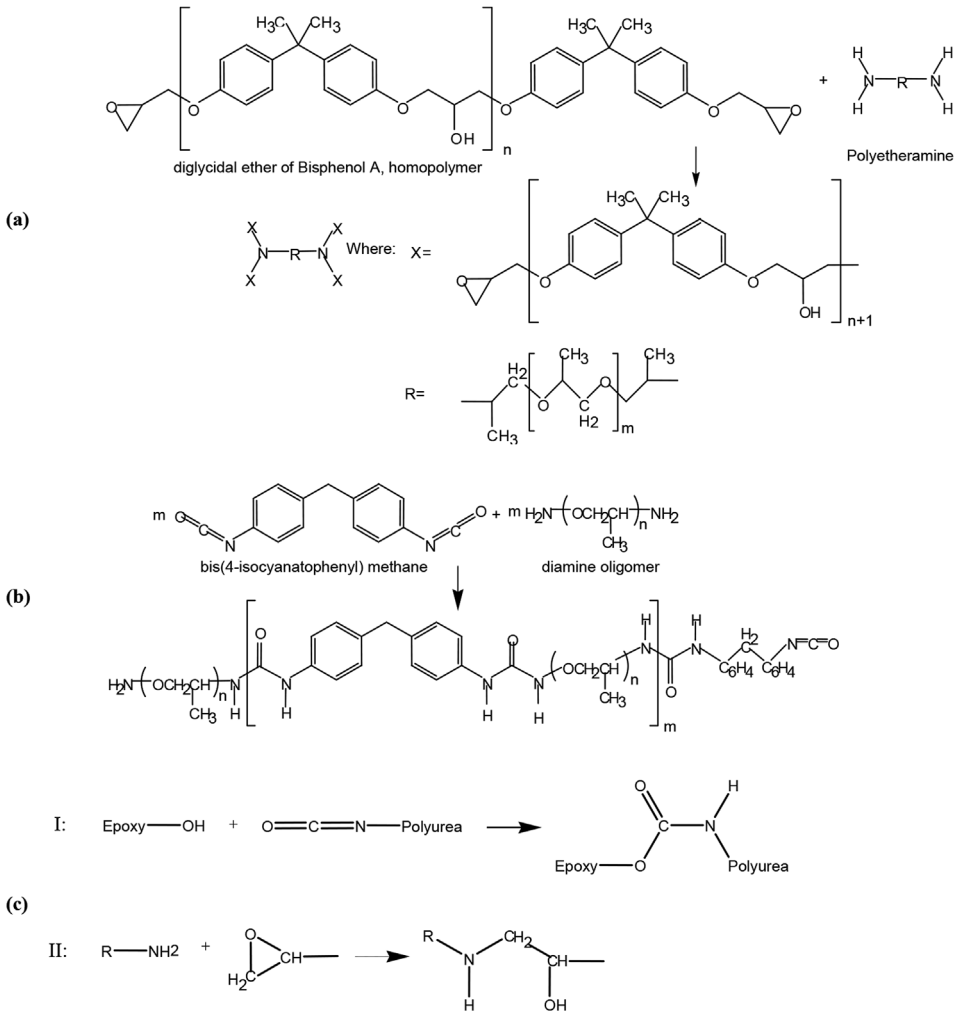

Fig. 2. The reaction schemes of: (a) the curing reaction of epoxy resin to form a 3-D highly cross-linked structure; (b) the polymerization reaction to form polyurea; (c) The suggested polyurea-epoxy reactions.

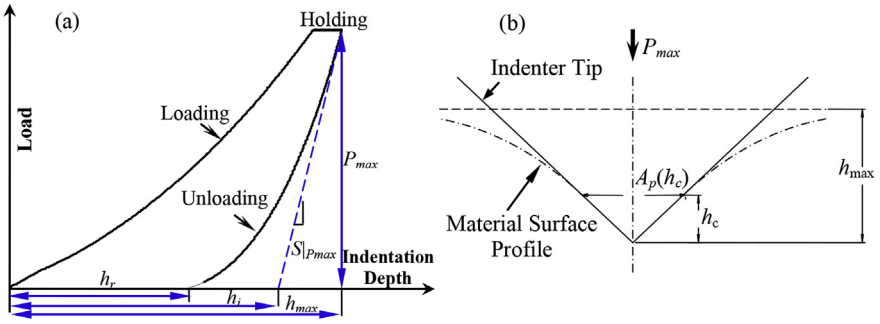

Fig. 3. Nanoindentation tests: (a) a sample load-indentation depth curve; (b) parameters used to analyze nanoindentation test results.

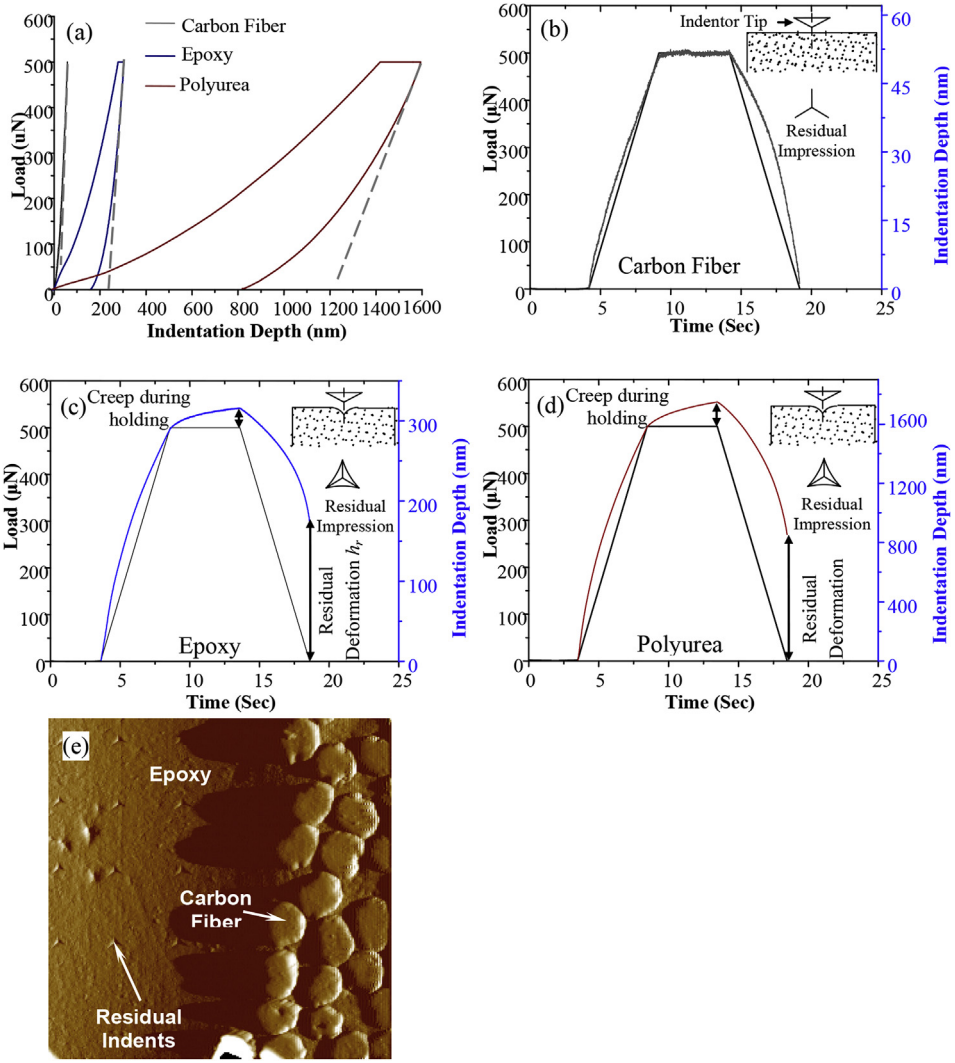

Fig. 4. (a) Typical indentation responses for the three primary phases in CHMC (load-indentation depth relationships); the load and deformation time-histories of (b) carbon fiber; (c) epoxy; (d) polyurea; and (e) AFM image showing the carbon fiber and epoxy surfaces after the nanoidentation tests.

constituent phases that comprise CHMC are presented in Fig. 4(a), and the displacement time-histories of carbon fiber, epoxy-based polymeric phase I, and elastomeric phase II, together with the load-time histories for each test are presented in Fig. 4(b)–(d), respectively. For an ideally-elastic solid, the sample surface deforms elastically during loading-and-unloading process. Upon load removal, impressions made by the indentor tip are fully recovered, leaving no traceable residual impressions on the sample surface. In comparison, an elasto-plastic solid deforms both elastically and plastically upon loading. The elastic deformation component recovers during the unloading process; however, the plastic component of the deformation is permanent [24,25], leaving a partially recovered impression mark as shown in Fig. 4(c) and (d). In addition, the indentation curves of materials exhibiting time-dependent behavior, e.g., polymers, elastomers, or bitumen, may exhibit viscoelastic or viscoplastic characteristics, leading to a creep plateau during the holding stage, see Fig. 4(c) and (d) [26]. The indentation curves of carbon fiber show high elastic modulus and very little plastic deformation; the epoxy-based matrix phase I exhibit a mediate level of plastic deformation, as indicated by the residual deformation on the load-indentation curve and the residual impression as shown in

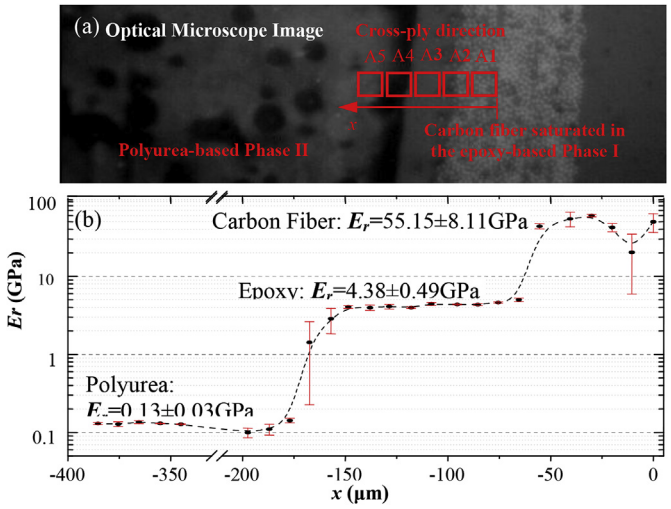

Fig. 5. (a) The optical microscopy image showing the cross-ply profile; (b) the cross-ply modulus profile determined using nanoindentation.

Fig. 4(e); and the polyurea-based matrix phase II shows a significantly greater level of plastic/viscoplastic deformation than both the carbon fiber and the epoxy. As far as the time-dependent properties of the three constituents are concerned, deformation caused by material creep during the 5-s holding stage is signified by the plateau encountered at maximum load. Carbon fiber shows almost no viscous component in its deformation diagram, see Fig. 4(a). The deformation time-history response presented in Fig. 4(b) appears to be consistent with this observation. On the other hand, the two polymeric phases both exhibit certain levels of viscoplastic behavior.

3.2. Elastic properties

In order to determine the elastic properties of materials along the cross-ply direction, the nanoindentor was programmed to analyze a five by five indent matrix (twenty-five tests) within each of five selected indentation regions, see the red boxes in Fig. 5(a), where the spacing of each row and column within each region was 25 μm. The indentation tests were load-controlled to 500 micro-Newtons (μN) at constant load rate; the maximum load of 500 μN was held for 5 s before being unloaded. The reduced moduli of the three primary constituents were calculated based on Equation (6) using the indentation results. The stiffness profile along the cross-ply direction of the CHMC laminate is plotted in Fig. 5(b), where the average stiffness in the reinforcing fibers transitions from 55.15 GPa to 4.39 GPa for the epoxy-based matrix phase I to 0.13 GPa for the polyurea phase II, also see Table 1. Transitions in the elastic moduli are observed across the fiber-epoxy and epoxy-polyurea interfaces, where Fig. 5(b) shows a gradual transition from stiffness of the epoxy matrix to stiffness of the polyurea matrix. The existence of new polymer is identified at the interface within region A4.

Table 1
Nanoindentation results - Reduced Modulus E_r.

	# of indents	Mean	Min	Max	Std. Dev.
		(GPa)			
Polyurea	41	0.130	0.0812	0.2737	0.0304
Polyrea-epoxy interface	4	1.041	0.1511	1.8601	0.9225
Polymeric Phase I	47	4.385	3.5066	6.0390	0.4945
Fiber-epoxy Interface	6	27.621	13.778	37.711	10.691
Carbon Fiber	18	55.153	40.332	71.850	8.1182

4. Dynamic properties and damping characterization of CHMC beams

4.1. Analysis of multi-layered composite beams

For viscoelastic beams subjected to harmonic loading at frequency ω, the complex material modulus may be expressed as:

$$E_\omega^* = E_\omega'(1 + i\eta_\omega) \tag{3}$$

where η_ω is the loss factor that relates the storage modulus E_ω' (which can include the dynamic Young's modulus as a function of ω_i), see Equation (4), to the loss modulus E_ω'', i.e., indicating the amount of stored energy (before unloading occurs) relative to the amount of energy dissipated via heat.

$$E_\omega' = \frac{\omega_i^2 L^4}{[(2i+1)\pi]^4}\frac{\rho A}{I} \tag{4}$$

where A and I are the area and moment of inertia of the beam cross-section, respectively; ρ is the mass density; and i is the mode. The loss modulus, E_ω'', may be calculated using the storage modulus and or the loss factor via Equation (3) as:

$$E_\omega'' = E_\omega' \tan\eta_i \approx 2E_\omega'\xi_i \tag{5}$$

where ξ_i is the damping coefficient of mode i.

For layered materials comprised of a damping layer and elastic layer, the flexural moduli and loss factors may be estimated using the Ross-Kerwin-Ungar (RKU) equations [1]. In a simple case of unconstrained or free-layer damping treatment (Fig. 6 (a)), the flexural modulus and loss factor may be expressed as:

$$\frac{EI}{E_1 I_1} = \frac{1 + 4eh + 6eh^2 + 4eh^3 + e^2h^4}{1 + eh} \tag{6}$$

$$\frac{\eta}{\eta_2} = \frac{eh(3 + 6h + 4h^2 + 2eh^3 + e^2h^4)}{(1 + eh)(1 + 4eh + 6eh^2 + 4eh^3 + e^2h^4)} \tag{7}$$

where $e = E_2/E_1$, $h = H_2/H_1$, and E_1 and E_2 represent the storage moduli (E_ω') of Materials 1 and 2 in Fig. 6 (a). Equations (4) and (5) apply to an extensional damping treatment where a layer of polyurea damping material is bonded to the underlying CF/E composite beam layer that is vibrating primarily in a bending mode, Fig. 6 (a); in this case, the term "polyurea" includes the epoxy-polyurea interface layered with pure polyurea coating. Implicit in this method is that shear deformation within the interface is ignored, thus, Equations (6) and (7) may not be accurate for CHMC when t_c is small, resulting in a relatively compliant high-damping interfacial layer, see Fig. 1(f). To consider the deformation of an epoxy-polyurea interface, see Fig. 6(b), the RKU equation for a three-layered laminated system may be used by considering the thickness and damping properties of the interfacial layer [1].

4.2. Specimen configurations and experimental setup

In order to quantify the damping properties of CHMC composite beams, either as self-standing composite laminates or as retrofitting materials for structural substrates, a series of vibration tests were conducted on beam specimens. The experimental setup is shown in Fig. 7(a) and Fig. 7(b). The specimens are supported horizontally in a clamped-clamped (fixed-fixed) condition, and a laser vibrometer was used to measure velocity time-histories of the test beams. Three types of beams, comprising 20 beam specimens, were tested to calculate damping properties of CHMC and their carbon fiber/epoxy (CF/E) counterparts, which include (*i*) 4 homogenous (self-supporting) beam specimens (Type I); (*ii*) 6 Oberst-type beam specimens, where damping materials (i.e., CF/E or CHMC) were attached to one side of a metal beam (Type II), and (*iii*) 10 modified Oberst-type beam specimens, where damping materials were attached symmetrically to both sides of

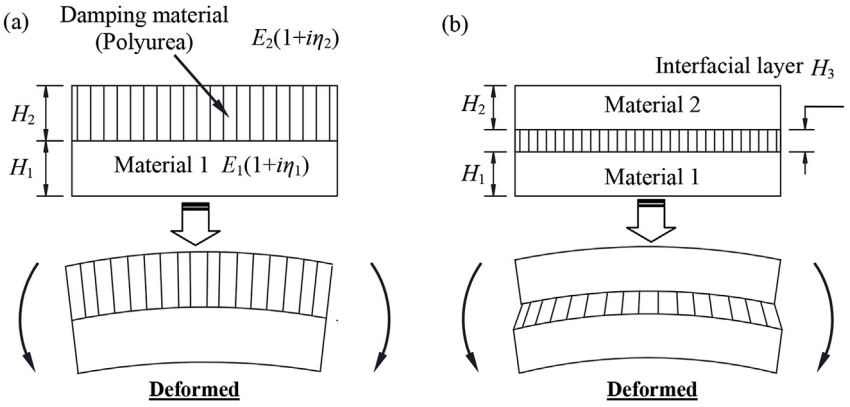

Fig. 6. Deformation of layered composite materials with (a) unconstrained free-layer damping material; and (b) compliant interfacial layer with significant material damping.

a metal base beam (Type III) were tested. The Oberst and modified-Oberst beams were tested to examine CHMC as the retrofitting/strengthening material to a substrate structure where polyurea can be applied only on one side of the composite. The three types of specimens are shown schematically in Fig. 7(c). The composite laminates were prepared via a hand lay-up process using Torayca® unidirectional carbon fiber fabric having a nominal single-ply thickness of 0.33 mm, and the epoxy resin was produced by BASF. The material properties are reported in the manufacturer's data sheets [27,28]. Forced vibration tests were performed using an electromagnetic shaker. Banded white-noise excitations with peak acceleration amplitudes of 0.3 g and 3 g were used to excite beam specimens. Two accelerometers were mounted on the shaker base to ensure that the actual excitation signal complied with the desired input signal.

4.3. Data processing and reduction

The free vibrations of the beams were excited using pulse loading induced by a hammer, Fig. 8(a). The beam responses were recorded and then processed to obtain both the response time-histories, Fig. 8(b), and the frequency spectra, Fig. 8(c), for each excitation. The damping coefficient, ξ, may be evaluated experimentally using the logarithm decrement method (when analyzing free response data in time domain) via Equation (8):

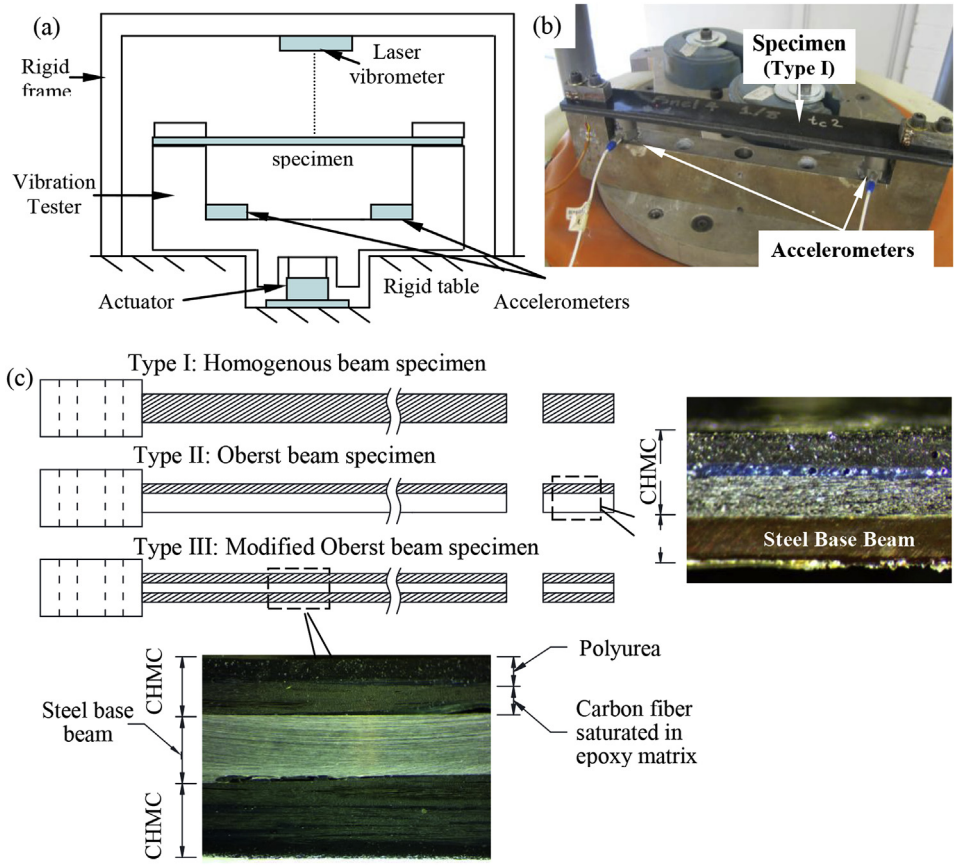

Fig. 7. Experimental setup and specimen configurations (a) illustrative figure showing the test setup; and (b) picture showing the test setup and instrumentations; and (c) specimen configurations.

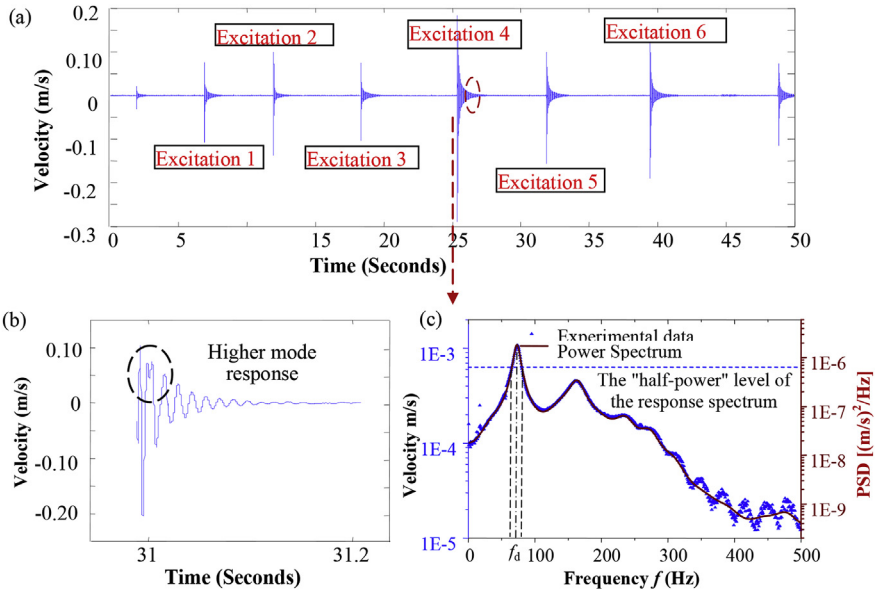

Fig. 8. Responses of a free vibration test: (a) raw data; and (b) extracted time-history response; and (c) the velocity spectrum and PSD of a free vibration.

$$\xi = \left[\frac{1}{\omega_1(n-1)T_d}\right]\ln\frac{x_1}{x_n} \tag{8}$$

where x_1 are x_n are amplitudes of the first and nth vibration cycles used in a logarithm decrement calculation; ω_1 is the natural frequency of the first mode of vibration expressed in rad/sec; and T_d is the period of vibration of the first cycle of the damped response.

When analyzing responses in the frequency domain, e.g., using the power spectrums, loss factors, η_i, may be calculated using the half-power bandwidth method [29] to normalize the power at each frequency content via Equation (9):

$$\eta_i = \frac{\Delta f_i}{\Delta f_{0,i}} \tag{9}$$

where $f_{0,i}$ is the natural frequency (Hz) of mode i, and $\Delta f = f_2 - f_1$ is the frequency difference between half-power points. For forced vibration tests, a limited bandwidth white noise excitation signal is used to excite the specimen, Fig. 9(a), and the corresponding response is recorded using a laser vibrometer. Measured time-history responses may then be converted into frequency spectrums via Fast Fourier Transformation (FFT), and power spectral density (PSD) distributions, which quantify the power in the response per unit frequency, were estimated using the Yule-Walker autoregressive method [30], see Fig. 9(b). Loss factors for each vibration mode are determined via the half-power bandwidth method.

5. Results and discussion

5.1. Flexural stiffness

The homogenized equivalent flexural modulus of the composite laminates can be estimated using the laminate profile and elastic properties as determined in Section 3 based on the RKU equations [1]. Table 2 compares the flexural modulus estimated using the constituent's properties tested by nanoidentation tests and the RKU equations with the elastic moduli measured by vibration tests, where h_f, h_{m1}, and h_p indicate the equivalent thicknesses of the carbon fiber, epoxy, and polyurea layers, respectively. E'_{meas} is the flexural modulus computed using the measured beam dynamic properties.

The error between measured flexural modulus and modulus calculated was calculated using the RKU equations. A good match (within 15%) is found between measured and calculated moduli for homogenous (Type-I specimens). The large discrepancy between measured and calculated values of Oberst (Type II) beams, specimens #8 - #9, explains how the calculated elastic modulus and loss factor, Equations (4) and (5), does not account for the epoxy-polyurea interfacial layer, see Figs. 6(b), 10(c) and 10(d), which provides additional stiffness and damping as will be discussed later. Non-uniformity of the cross-section along the specimen length, due to specimen preparation error, elicits additional error. For the modified Oberst Beams, large discrepancies are observed between predicted results and measured modulus for specimens #16 - #20, in which cases thicker base beams (1.32 mm) were used. Since the analysis of the symmetric free layer (or Modified Oberst)

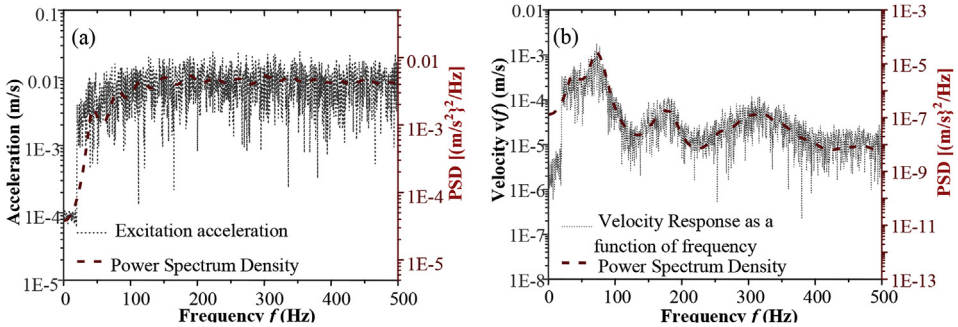

Fig. 9. Sample data showing the velocity spectrum and PSD of a forced vibration test: (a) the white noise excitation signal used for the tests; (b) beam response (frequency domain).

Table 2
The moduli measured by vibration tests as compared to the model prediction.

Spec#	Mater. Type	Test Type	t_c	h_f	h_{m1}	h_p	$E'_{meas.}$	$E_{calc.}$	err
			hr.	mm	mm	mm	GPa	GPa	%
1	CF/E	Homo. Beams (Type I)	n.a.	0.330	0.708	n.a.	5.065	5.704	12.62
2	CHMC		2.5	0.456	0.384	3.435	0.195	0.180	8.05
3			3.5	0.456	0.384	3.325	0.179	0.154	13.93
4			4.5	0.456	0.384	3.158	0.164	0.162	1.48
5	CHMC	Oberst Beams (Type II)	2.5	0.550	0.384	1.765	1.866	1.700	8.89
6			3.5	0.550	0.384	1.012	3.976	3.546	10.80
7			4.5	0.550	0.384	0.499	7.870	7.213	8.36
8			2.5	0.550	0.384	1.575	3.160	1.991	36.99
9			3.5	0.550	0.384	0.829	7.585	4.463	41.16
10			4.5	0.550	0.384	0.625	5.888	5.932	0.75
11	CF/E	Modified Oberst Beams (Type III)	n.a.	0.550	0.306	n.a.	32.438	25.146	22.48
12	CHMC		2.5	0.550	0.384	0.889	4.937	4.129	16.37
13			3.5	0.550	0.384	0.614	7.053	6.036	14.42
14			2.5	0.550	0.384	1.415	3.883	2.305	40.64
15			3.5	0.550	0.384	1.437	1.938	2.258	16.54
16	CF/E		n.a.	0.550	0.333	n.a.	35.562	22.456	36.85
17	CHMC		2.5	0.550	0.384	0.889	12.235	4.129	66.26
18			3.5	0.550	0.384	0.582	19.842	6.332	68.09
19			2.5	0.550	0.384	1.894	8.117	2.257	72.19
20			3.5	0.550	0.384	1.493	11.563	3.332	71.19

beams is based on Euler-Bernoulli beam theory, attention must be given when using Equations (11) and (12) if the retrofitting laminate thickness is not much greater (about 4 times) than that of the metal beam [1,31].

5.2. Free-vibration response

For the homogenous beams in Fig. 7(c) - Type I, loss factors of sample materials were directly obtained using the beam responses according to Equation (9), and the dynamic Young's modulus of the homogenized beam may then be estimated using the modal frequency via Equation (3). Fig. 10(a) shows the example free-vibration velocity

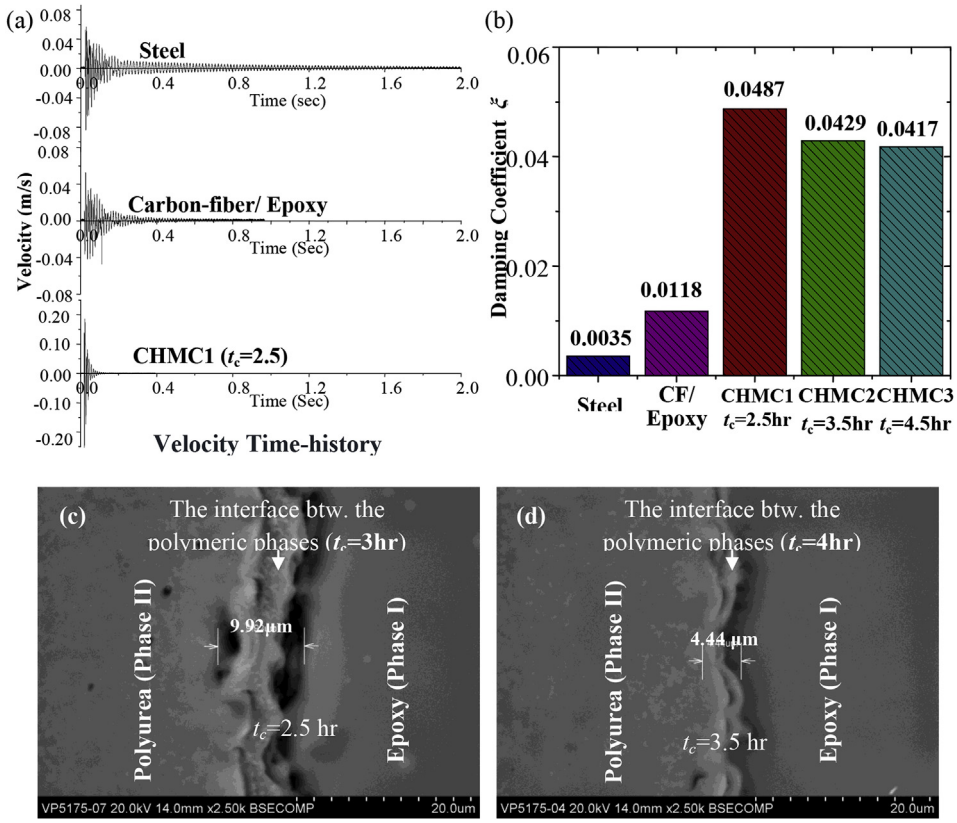

Fig. 10. (a) Time-history responses of steel, carbon fiber reinforced epoxy, and CHMC beams under free vibration; (b) damping coefficient calculated from the free vibration responses; The interface morphology as a function of t_c (c) t_c = 2.5hr.; (d) t_c = 3.5hr.

responses of steel, CF/E, and a CHMC (processed at t_c = 2.5 hrs) beam. It is evident from the velocity time-history responses of CHMC beams that the peak-to-peak response per cycle diminished substantially quicker than peaks of CF/E and steel beams. The first-mode damping coefficients for steel, CF/E, and three types of CHMC beams (processed at t_c = 2.5 hrs, t_c = 3.5 hrs, and t_c = 4.5 hrs to show that the damping decreases at higher t_c even as h_p increases) are plotted and compared in Fig. 10(b). It is observed that damping coefficient minimally decreases as elapsed curing time of the epoxy, t_c, increases in accordance with the generation of the hybridized interface. Fig. 10(c) and (d) present different widths and morphology for two polymeric interfacial regions (between epoxy and polyurea phases) generated from two t_c values. However, Dynamic Mechanical Analysis (DMA) reveals that lower t_c substantially increases damping, attributing crosslinking density of the interface following timely reaction of epoxy functional groups and pre-polymerized polyurea functional groups, Fig. 2(c). Therefore, designing a wider and more "chemically bond rich" interface engenders greater internal cohesion and molecular vibrational properties, netting greater bond stretching and rotation [32], and larger damping in CHMC.

5.3. Forced-vibration response

The forced vibration responses of homogenous beams (Type I) are obtained by exciting the beam specimens using a limited band-width white noise. Fig. 11 presents the power spectral density (PSD) curves of the beams manufactured from steel, CF/E, and CHMC1 (t_c = 2.5 h) using an excitation PEA = 0.3 g. It is evident from Fig. 11 that under the same excitation condition, energy contained in the velocity response signal of the CHMC beam is significantly lower relative to energies in the steel and CF/E beams, especially at higher modes of vibration. Suppression of higher modes can be critical in certain higher-frequency-sensitive applications. Using the first three vibration modes of CF/E and three CHMC beams (CHMC1, CHMC2, and CHMC3, see Fig. 9(b)), frequencies found from PSD distributions (Figs. 7b and 8b), loss factors and modal damping coefficients calculated using the half-power bandwidth method, as described, are shown in Table 3. There is an ostensible dependency of modal damping coefficient to epoxy curing time, t_c; a similar trend is observed in the free vibration test results (for the first three vibration modes), i.e., damping coefficients tend to increase as t_c decreases. Although there is no consideration of h_p presented in Table 3, the dependency of damping relative to t_c (and not h_p) is increasingly apparent at higher excitation frequencies and at lower t_c. However, even for higher t_c, PSD distributions in Fig. 11 illustrate a broadening of spectrum peaks at higher vibration modes as a result of larger damping induced at a higher frequency range (for the same h_p, i.e., same samples).

Analysis of Oberst-type beams, i.e., steel base-beam with a composites laminate (either CHMC or CF/E) attached to one side, see Fig. 7(c) Type II, follows classical Euler-Bernoulli beam theory, where rotational inertia and shear deformation are neglected [1,32]. The dynamic

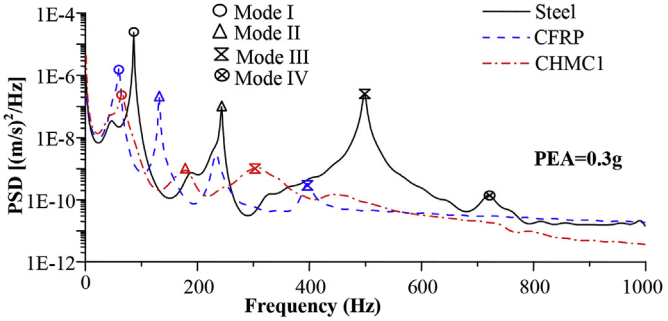

Fig. 11. Forced vibration test results of self-supporting beams: PSD obtained for steel, carbon fiber/epoxy, and CHMC beams (PEA = 0.3 g).

Table 3
Modal frequencies and damping coefficients of the first three vibration modes.

Spec#	Mater. Type	t_c	f_{n1}	f_{n2}	f_{n3}	ξ_1	ξ_2	ξ_3
		hr.	Hz	Hz	Hz			
1	CF/E	n.a.	57.495	131.470	232.544	0.012	0.013	0.012
2	CHMC	2.5	64.453	175.415	309.814	0.049	0.058	0.063
3		3.5	71.777	176.880	316.040	0.043	0.055	0.061
4		4.5	78.369	164.063	294.800	0.042	0.057	0.056

Young's modulus of the metal base-beam and the composite materials (CF/E or CHMC) are denoted as E_b and E, respectively; thickness of the base-beam and laminate are H_b and H, see Fig. 7(c). Modal frequencies of the Oberst beam and steel base beam are $\omega_{c,i}$ and $\omega_{1,i}$, respectively. Denoting loss factors of the Oberst beam and attached composite material as η_1 and η_2, Young's modulus and loss factors of the attached CHMC or CF/E laminate are computed using measured values of the composite Oberst beam, see Equations (4) and (5). Rewriting Equation (4) leads to Ref. [1]:

$$\left(\frac{f_{c,i}}{f_{1,i}}\right)^2(1+h\rho_r)=\frac{1+4eh+6eh^2+4eh^3+e^2h^4}{1+eh} \tag{10}$$

where $\rho_r = \rho_2/\rho_1$ is the density ratio of the tested composite material and metal beam.

Note that Young's modulus of the composite laminate, E, refers to a homogenized equivalent modulus which treats the laminate as a homogenous material. First-mode resonant frequencies and damping coefficients of the composite beam, f_c and ξ_c, and base beam, f_1 and ξ_1, together with the calculated damping coefficient of the retrofitting laminate, ξ_1, based on Equation (5) for each Oberst beam specimen, are summarized in Table 4. Damping coefficients of CHMC used as a retrofitting laminate are lower than the self-standing laminate because of the constraint of the base beam and because Oberst beams include epoxy-polyurea interface on only one side. The damping coefficients as functions of frequency of the CHMC-retrofitted beams follow a similar trend as the homogenous specimens, where damping increases as frequency increases.

For modified Oberst type specimens, i.e., CF/E and CHMC materials are symmetrically attached to metal base beams (see Fig. 7(c) - type III), the dynamic Young's modulus and loss modulus of the attached laminate may be expressed as functions of the properties of the composite beam and steel base beam as [1]:

$$E_2=\frac{[(f_{c,i}/f_{1,i})^2(1+2h\rho_r)-1]E_1}{8h^3+12h^2+6h} \tag{11}$$

$$\eta_2=2\xi=\eta_c\left[1+\frac{E_1}{E_2(8h^3+12h^2+6h)}\right] \tag{12}$$

where E_1 and E_2 are Young's modulus of the steel base beam and composite layers under test, respectively.

The damping coefficients were also evaluated using modified Oberst-type beams (Table 5), indicating similar results as for the

Table 4
Test results obtained using the Oberst beam specimen.

Spec#	Mater. Type	t_c	h_p	f_{c1}	f_{b1}	ξ_{c1}	ξ_{b1}	ξ_1
		hr.	mm	Hz	Hz			
5	CHMC	2.5	1.765	115.356	60.059	0.014	0.006	0.018
6		3.5	1.012	121.216	60.059	0.011	0.006	0.014
7		4.5	0.499	140.625	60.059	0.006	0.006	0.008
8		2.5	1.575	153.809	60.059	0.011	0.006	0.013
9		3.5	0.829	164.429	60.059	0.009	0.006	0.012
10		4.5	0.625	116.455	60.059	0.010	0.006	0.013

Table 5
Test results using the modified Oberst-beam specimen.

Spec#	Mater. Type	t_c	h_p	f_{c1}	f_{b1}	ξ_{c1}	ξ_{b1}	ξ_1
		hr.	mm	Hz	Hz			
11	CF/E	n.a.	n.a.	191.162	60.059	0.009	0.006	0.010
12	CHMC	2.5	0.889	152.344	60.059	0.015	0.006	0.016
13		3.5	0.614	156.738	60.059	0.018	0.006	0.019
14		2.5	1.415	166.260	60.059	0.017	0.006	0.018
15		3.5	1.437	123.047	60.059	0.015	0.006	0.017
16	CF/E	n.a.	n.a.	172.852	87.524	0.007	0.007	0.009
17	CHMC	2.5	0.889	174.683	87.524	0.012	0.007	0.015
18		3.5	0.582	192.993	87.524	0.011	0.007	0.012
19		2.5	1.894	183.838	87.524	0.016	0.007	0.019
20		3.5	1.493	189.331	87.524	0.012	0.007	0.014

homogenous (Type-I) and Oberst (Type-II) beams, where lower t_c (at smaller h_p) tends to increase damping; however, at $t_c = 3.5$ hrs, the damping coefficient (ξ) is greater than ξ at $t_c = 2.5$ hrs using similar Phase II polyurea thickness ($h_p = 1.437$ mm and 1.415 mm, respectively). In comparing the two modified Oberst (Type III) beams manufactured using $t_c = 3.5$ hrs, the use of thicker PU in the Type-III beams appears more critical towards increasing damping. However, this last result may not be relevant because analysis of (symmetric) Type-III beams assuming plane sections remain plane and using Equations (11) and (12) is limited by the thickness ratio, h, [1,32]. In the case of the modified Oberst beams herein, the laminate thickness (h_2) is much larger than that of the metal beam (h_1), with h ranging between 0.92 and 2.67. As a result, application of equations (11) and (12), which assume that plane sections are plane, to calculate the modulus and damping may not be valid. The modal damping coefficient, storage and loss moduli of CF/E and CHMC specimens obtained through the Oberst and modified Oberst type tests are plotted in Fig. 12.

5.4. Dynamic mechanical analysis of the epoxy-polyurea interface

Material damping is a critical property introduced in CHMC for a properly designed epoxy-polyurea interfacial reaction, where lower values of t_c are used. Although lower values of t_c were not examined in the Oberst (Type II) and modified Oberst (Type III) beam tests, resulting in lower calculated damping properties, dynamic mechanical analysis (DMA) of coupon-scale test specimens (30 mm × 7 mm x 5 mm) of 0-HMC reveals a strong correlation between t_c, material damping, and tan (δ), which is the ratio of loss modulus to storage modulus, see Fig. 13(a) and (b). In this study, "0" means no fiber, i.e., the specimen consists of polyurea of thickness h_p (in pre-polymerized form) applied to a thin layer of curing epoxy. A comparison of loss modulus for various values of t_c in 0-HMC test specimens (which are also influenced by epoxy and polyurea layers) and in just the interfacial region (region between epoxy and polyurea) reveals that in the latter, Fig. 13(b), loss modulus is over 100% greater for interfaces designed with $t_c = 0$ as opposed to $0.5 < t_c < 2$. The difference is even greater when comparing $t_c = 0$ interfaces and $t_c > 2$ interfaces.

The ratio of loss modulus to storage moduli, i.e., tan (δ), measures overall energy transferability in materials [33] as a function of material damping (which is proportional to loss modulus), inelastic material behavior (post-yield stiffness degradation), load-rate (ω), and elastic stiffness. Examination of tan (δ) in Fig. 14(a) and (b) reveals that tan (δ) is largest for $t_c = 0$ for both 0-HMC specimens as well as when only the interface (i.e., without epoxy or polyurea) is considered. However, there appears to be a smaller disparity when comparing tan (δ) for

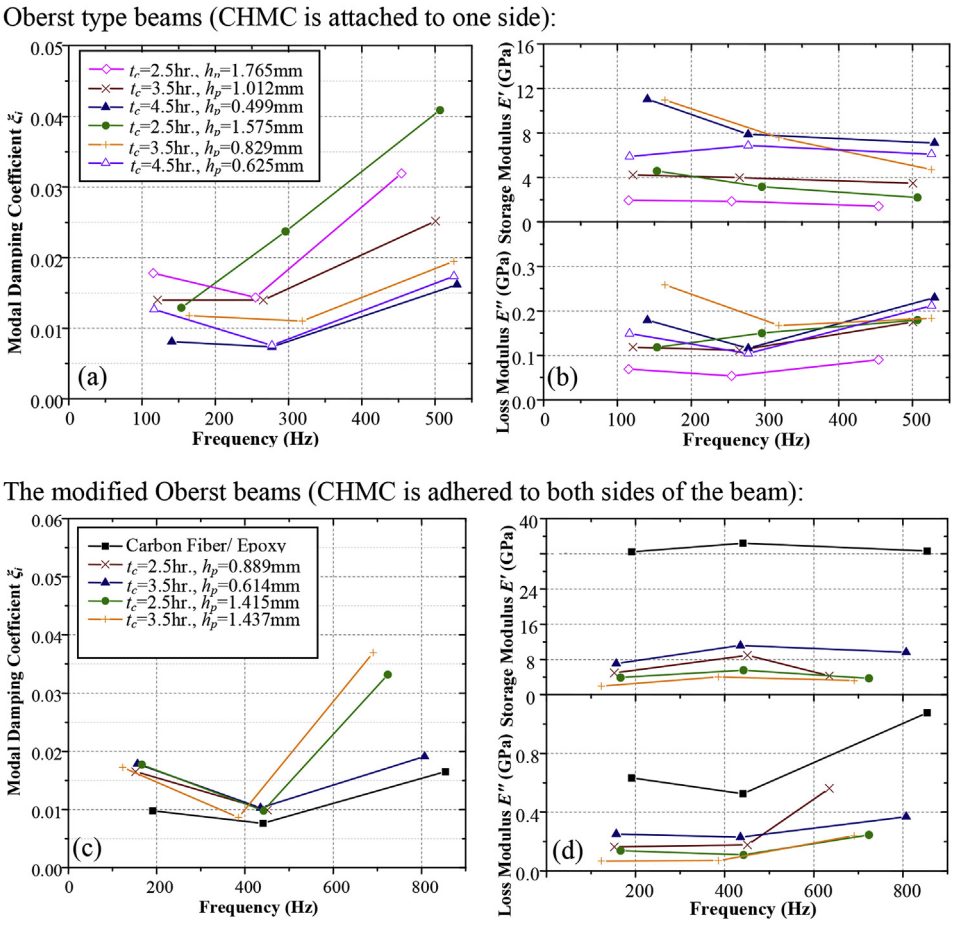

Fig. 12. The dynamic properties of CHMC obtained from Oberst and modified Oberst beams: (a) damping coefficients (Oberst-type beams); (b) storage and loss moduli as functions of frequency (Oberst-type beams); (c) damping coefficients (modified Oberst-type beams); (d) storage and loss moduli as functions of frequency (modified Oberst-type beams).

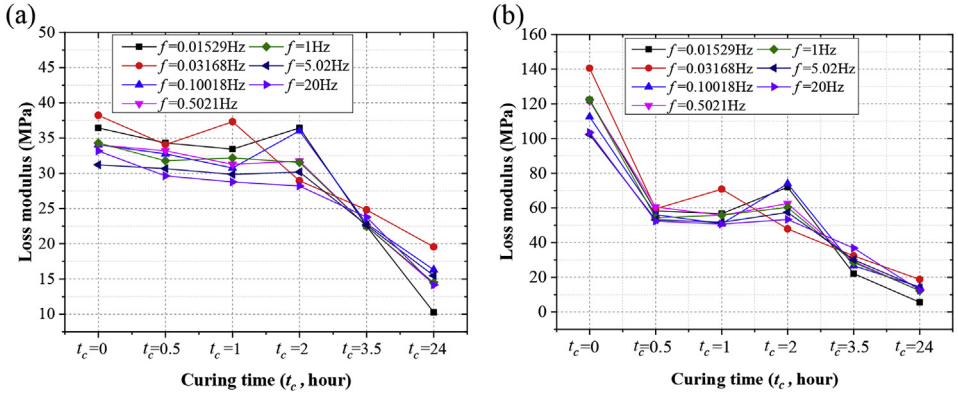

Fig. 13. Loss modulus via DMA of (a) 0-HMC specimens; and (b) epoxy-polyurea interface.

various t_c, Fig. 14(b), than the disparity in loss modulus, Fig. 13(b), when considering only the interface. However, given that specimen loading during DMA, see Fig. 15, did not induce material damage (inelasticity), there exists similarity between tan (δ) values for 0-HMC, Fig. 14(a), and only the interface, Fig. 14(b), due to substantial storage modulus (via elastic stiffness) elicited by a likely interfacial reaction of epoxide + NH_2 (from epoxy) + (−NCO), providing necessary stress transferring paths in the carbon-fiber/matrix system within CHMC. However, the substantial loss modulus, Fig. 13(b), also provided by the interface, is essential to mechanical energy transfer via the unique covalent chemistry (bond strength/enthalpy and molecular vibrations), which minimizes fiber damage, and ingenerates resiliency and overall composite strength sustainability. These findings are consistent with previous studies [22], where epoxy-polyurea interface width decreases as t_c increases, see Fig. 10(c) and (d), and where there is no interfacial chemical reaction or physical region in specimens manufactured using fully cured epoxy.

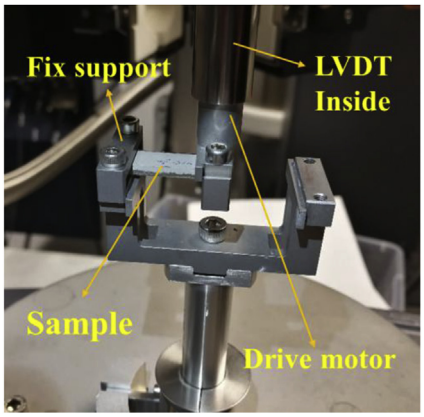

Fig. 15. Setup of the dynamic mechanical analysis test.

6. Conclusions

This paper presents the development and properties of a new Carbon-fiber reinforced epoxy-polyurea Hybrid Matrix Composite (CHMC), which has superior damping properties over conventional carbon-fiber reinforced epoxies (CF/E), for vibration suppression applications. Scanning electron microscopy (SEM) images show the various microstructures, morphologies, and multilayer cross-ply textures of CHMC. Micromechanical properties of the constituents are studied using nanoindentation test, and the cross-ply modulus profile of various types of CHMC laminates are obtained. Nanoindentation test results indicate substantial damping properties in accordance with the matrix constituents, where the crosslinking reaction of the curing epoxy phase is altered via addition of polyurea in pre-polymerized form, i.e., in its reactive state. The interfacial reaction between curing epoxy and polyurea produces strong cohesion and material damping in CHMC.

The methodology used to characterize the dynamic performance and damping property of composite materials is presented and discussed. Dynamic properties of CHMC and conventional CF/E are investigated using free vibration and forced vibration testing. Natural frequencies and damping coefficients are calculated using velocity time-histories/vibration responses of various test beams. CHMC exhibits significantly greater damping and vibration suppression capability than conventional CF/E both as a stand-alone structural material and as part of a retrofitting solution. Furthermore, material damping in CHMC appears to be larger when used as a stand-alone laminate versus retrofitting material. The influence of two material processing parameters – t_c and h_p – on material damping has also been investigated,

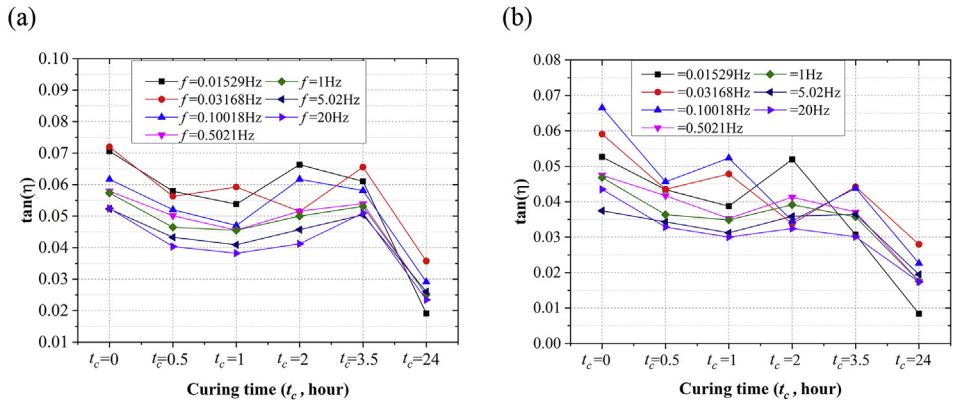

Fig. 14. Loss factor, tan(δ), obtained via DMA for: (a) 0-HMC (via DMA); and (b) interface, i.e., the region between epoxy and polyurea.

where dynamic mechanical analyses (DMA) clearly shows substantial loss modulus, related to material damping, in epoxy-polyurea chemical regions designed with small epoxy curing times (t_c).

Acknowledgements

This research was partially supported by the Department of Homeland Security through the Higher Education Research Experience (HERE) Program, and the Southeast Region Research Initiative (SERRI) at the Department of Energy's Oak Ridge National Laboratory (ORNL), DHS Project No. 90300 and Alabama Department of Transportation (Project 930-921). The authors also would like to thank Professor Marc Mignolet and Dr. Raghavendra Murthy for their assistance in testing the beam specimens used in this study.

Appendix A. Supplementary data

Supplementary data to this article can be found online at https://doi.org/10.1016/j.compositesb.2019.01.064.

References

[1] Nashif AD, Jones DIG, Henderson JP. Vibration damping. New York, NY: Jonh Wiley & Sons; 1985.
[2] Berthelot JM, Sefrani Y. Damping analysis of unidirectional glass and Kevlar fibre composites. Compos Sci Technol 2003;64:1261–78.
[3] Le Guen MJ, Newman RH, Fernyhough A, Emms GW, Staiger MP. The damping-modulus relationship in flax-carbon fibre hybrid composites. Compos B Eng 2016;89:27–33. https://doi.org/10.1016/j.compositesb.2015.10.046.
[4] Treviso A, Van Genechten B, Mundo D, Tournour M. Damping in composite materials: properties and models. Compos B Eng 2015;78:144–52. https://doi.org/10.1016/j.compositesb.2015.03.081.
[5] Adams RD, Fox MAO, Flood RJL, Friend RJ, Hewitt RL. The dynamic properties of unidirectional carbon and glass fiber reinforced plastics in torsion and flexure. J Compos Mater 1969;3:594–603.
[6] Adams RD, Bacon DGC. Effect of fibre orientation and laminate geometry on the dynamic properties of CFRP. J Compos Mater 1973;7:402–28.
[7] Gibson RF, Plunkett R. Dynamic mechanical behavior of fiber-reinforced composites: measurement and analysis. J Compos Mater 1976;10:325–41.
[8] Suarez SA, Gibson RF, Deobald LR. Random and impulse techniques for measurement of damping in composite materials. Exp Tech 1984;6(2):10–4.
[9] Suarez SA, Gibson RF, Sun CT, Chaturvedi SK. The influence of fiber length and fiber orientation on damping and stiffness of polymer composite materials. Exp Mech 1986;26(2):175–84.
[10] Crane RM, Gillespie JW. Characterization of the vibration damping loss factor of glass and graphite fiber composites. Compos Sci Technol 1991;40:355–75.
[11] Hadi AS, Ashton JN. Measurement and theoretical modelling of the damping properties of a unidirectional glass/epoxy composite. Compos Struct 1996;34:381–5.
[12] Rajoria H, Jalili N. Passive vibration damping enhancement using carbon nanotube-epoxy reinforced composites. Compos Sci Technol 2005;65:2079–93.
[13] Khan SU, Li CY, Siddiqui NA, Kim JK. Vibration damping characteristics of carbon fiber-reinforced composites containing multi-walled carbon nanotubes. Compos Sci Technol 2011;71:1486–94.
[14] Ludwig T, Doreille M, Merazzi S, Vescovini R, Bisagni C. Dynamic finite element simulations of composite stiffened panels with a transverse-isotropic viscoelastic energy dissipation model. Prog Aero Sci 2015;78:30–8. https://doi.org/10.1016/j.paerosci.2015.06.001.
[15] Liu PF, Xing LJ, Zheng JY. Failure analysis of carbon fiber/epoxy composite cylindrical laminates using explicit finite element method. Compos B Eng 2014;56:54–61https://doi.org/10.1016/j.compositesb.2013.08.017.
[16] Hwang SJ, Gibson RF. The use of strain energy-based finite element techniques in the analysis of various aspects of damping materials and structures. J Compos Mater 1992;26:2585.
[17] Lakes RS. High damping composite materials: effect of structural hierarchy. J Compos Mater 2002;36:287–97. https://doi.org/10.1106/002199802023538.
[18] Tsai JL, Huang BH, Cheng YL. Enhancing fracture toughness of glass/epoxy composites by using rubber particles together with silica nanoparticles. J Compos Mater 2009;43:3107–23. https://doi.org/10.1177/0021998309345299.
[19] Cawse JL, Stanford JL. Rubber-toughened polyurethane network and composite materials. Polymer 1987;28:356–67. https://doi.org/10.1016/0032-3861(87)90186-8.
[20] Zhou H, Attard TL. Rehabilitation and strength sustainability of fatigue damaged concrete–encased steel flexural members using a newly developed polymeric carbon–fiber composite. Compos B Eng 2013;45:1091–103https://doi.org/10.1016/j.compositesb.2012.07.019.
[21] Zhou H, Attard TL, Wang Y, Wang J-A, Ren F. Rehabilitation of notch damaged steel beams using a carbon fiber reinforced hybrid polymeric-matrix composite. Compos Struct 2013;106:690–702https://doi.org/10.1016/j.compstruct.2013.07.001.
[22] Zhou H, Dhiradhamvit K, Attard TL. Tornado-borne debris impact performance of an innovative storm safe room system protected by a carbon fiber reinforced hybrid polymeric-matrix composite. Eng Struct 2014;59:308–19. https://doi.org/10.1016/j.engstruct.2013.10.041.
[23] Oliver WC, Pharr GM. An improved technique for determining hardness and elastic modulus using load and displacement sensing indentation experiments. Mater Res 1992;7:6–11.
[24] Yan W, Pun CL, Wu Z, Simon GP. Some issues on nanoindentation method to measure the elastic modulus of particles in composites. Compos B Eng 2011;42:2093–7. https://doi.org/10.1016/j.compositesb.2011.05.002.
[25] Yan W, Pun CL, Simon GP. Conditions of applying Oliver-Pharr method to the nanoindentation of particles in composites. Compos Sci Technol 2012;72:1147–52. https://doi.org/10.1016/j.compscitech.2012.03.019.
[26] Das B, Eswar Prasad K, Ramamurty U, Rao CNR. Nano-indentation studies on polymer matrix composites reinforced by few-layer graphene. Nanotechnology 2009;20:125705. https://doi.org/10.1088/0957-4484/20/12/125705.
[27] BASF. Mbrance CF 130 Data Guide. Shakopee, MN: BASF Construction Chemicals, LLC - Building Systems; 2007.
[28] BASF. Mbrace Primer Data Guide. Shakopee, MN: BASF, The Chemical Company; 2007.
[29] Rao SS. Vibration of continuous systems. New York, NY: John Wiley & Sons; 2007.
[30] Gersch W, Sharpe D. Estimation of power spectra with finite-order autoregressive models. IEEE Trans Automat Contr 1973;18:367–9. https://doi.org/10.1109/TAC.1973.1100350.
[31] ASTM E756-05. Standard test method for measuring vibration-damping properties of materials. West Conshohocken, PA: ASTM; 2010.
[32] Evans E, Ritchie K. Dynamic strength of molecular adhesion bonds. Biophys J 1997;72(4):1541–55.
[33] Chang M, Thomas D, Sperling L. Characterization of the area under loss modulus and tan δ–temperature curves: acrylic polymers and their sequential interpenetrating polymer networks. J Appl Polym Sci 1987;34(1):409–22.